

Plasmonic enhancement of single-molecule fluorescence under one- and two-photon excitation Lu. X.

Citation

Lu, X. (2021, December 8). *Plasmonic enhancement of single-molecule fluorescence under one- and two-photon excitation. Casimir PhD Series*. Retrieved from https://hdl.handle.net/1887/3245677

Version: Publisher's Version

Licence agreement concerning inclusion of doctoral

License: thesis in the Institutional Repository of the University

of Leiden

Downloaded from: https://hdl.handle.net/1887/3245677

Note: To cite this publication please use the final published version (if applicable).

4

Controlled synthesis of gold nanorod dimers with end-to-end configurations

End-to-end gold nanorod dimers provide unique plasmonic hotspots with extremely large near-field enhancements in the gaps. Thereby they are beneficial in a wide range of applications, such as enhancing the emissions from ultra-weak emitters. For practical purposes, synthesis of gold nanorod dimers with high yield, especially on the substrates, is essential. Here, we demonstrate two controllable strategies to synthesize gold nanorod dimers based on the self-assembly of gold nanorods, either in bulk solution or on the surface of a glass substrate directly. Both methods can give a high yield of gold nanorod dimers, yet, assembling them directly on the substrate provides more flexibility in controlling the shape and size of each nanorod within the dimer.

4.1. Introduction

Plasmonic coupling between metallic nanoparticles can strengthen the near-field enhancement inside the interparticle gaps[1–10], as well as the local density of photon states[6, 11–15], compared to individual nanoparticles. As a consequence, metal nanoparticle aggregates can be applied to enhance ultra-weak signals, such as two-photon-excited (TPE) fluorescence[16]. These TPE fluorescence signals are normally too weak to be detected at single-molecule level, particularly when single nanoparticles are used. Nanoparticle dimers provide single plasmonic hotspots without reducing the overall fluorescence enhancements. Therefore nanoparticle dimer structures can be considered as the best plasmon-coupling systems for single-molecule fluorescence enhancement in the sense that, i) they provide single sites for fluorescence enhancements, and ii) the photoluminescence background from the nanoparticles can be reduced compared to multimer aggregates.

Among all the metal nanoparticles, chemically synthesised gold nanorods (GNRs) with elongated shape have proven to be the excellent building blocks for constructing plasmonic dimers. Compared to spherical nanoparticles, the anisotropy of the GNRs gives rise to much richer flexibility in tailoring the optical responses of the dimer structures. GNRs support two surface plasmon modes along their transversal and longitudinal axes[17, 18]. The longitudinal plasmon resonance can be tuned from visible to the near-infrared region by varying the aspect ratio[17, 19, 20]. While two GNRs are placed adjacent to each other, the plasmon resonance can be further adjusted by the interparticle gap and by the relative orientation[21–24]. End-to-end GNR dimers are of particular interest as they produce higher near-field enhancement than other configurations as a result of the stronger coupling between the longitudinal modes. Preparation of end-to-end GNR dimers with high yield, especially on the substrate, is therefore beneficial for various plasmon-mediated applications[24, 25]. With this aim, various approaches have been developed to link the GNRs in an end-to-end fashion.

DNA origami templates can be used to assemble individual GNRs into well-defined nanoarchitectures[22, 26–28], including the end-to-end dimer[29–31], yet this approach requires harsh treatments to both the GNR suspensions and the DNA templates. A more straightforward approach is to link GNRs directly in an end-to-end fashion through electrostactic attraction[32, 33] or through covalent binding via molecular linkers[34–36]. Chemically synthesised GNRs are highly anisotropic in surface reactivity due to their anisotropic crystal structures, hence allow site-specific functionalization on the surfaces. For cetyltrimethylammonium bromide (CTAB) stabilized GNRs, for instance, the tips are more accessible to dithiol groups as the results of smaller population of CTAB[37, 38], which thus can trigger the end-to-end self-assembly of GNRs in the suspension[17]. For most cases, the dithiol ligands can serve not only as linkers, but also as spacers that separate the GNRs. Hence, dithiol ligands with different molecular sizes can be used to control the interparticle gaps of GNR assemblies[34, 39-41]. Despite the facilitation of end-to-end connections, controlled synthesis of GNR dimers with high yield in bulk suspension remains challenging because lack controls to stop the dimers from randomly growing into chain-like morphologies in the suspensions[34–36, 39–43].

Here, we have applied two strategies to synthesize end-to-end GNR dimers with the aid of biotinylated streptavidin as molecular linkers. Firstly, we illustrate the assembly in a bulk

suspension of GNRs in the presence of the biotinylated streptavidin. The biotinylated streptavidin can bind specifically to the tips of the GNRs in the presence of the surfactant CTAB, hence ensuring the end-to-end assemblies of the GNRs. The assembly was monitored by recording the extinction spectra of the assembly suspension over time, and a drop of this suspension was later deposited and dried between two glass slides. Secondly, we performed the GNR dimer assembly directly on glass slides. We first immobilized single nanorods on a clean glass slide, and functionalized them with the biotinylated streptavidin specifically on the tips of the each GNR. The molecular linkers functionalized on the immobilized gold nanorods have the chance of adsorbing a second GNR in the solution, hence forming dimer structures. During the assembly, based on the bottom-up flipped strategy, we can separate the inevitable multimer aggregates in the suspensions. Thereby we can get purified end-to-end GNR dimer structures on glass.

4.2. Materials and Method

4.2.1. Materials

The following chemicals and materials were used for the synthesis of the GNR dimers: Unconjugated streptavidin (SNN1001, invitrogen), N-[6-(biotinamido)hexyl]-3'-(2'-pyridyldithio) propionamide (EZ-link HPDP-biotin; Pierce), tris(2-carboxyethyl)phosphine) (TCEP, Pierce), Cetyltrimethylammonium bromide (CTAB), CTAB-stabilized Gold nanorods with plasmon resonance of 700 nm (NA-40-700, OD-50, Nanoseedz), Glass slides (Menzel-Gläser, $\phi=25~\mathrm{mm}$).

4.2.2. Methods

Figure 4.1 schematically illustrates the two assembly strategies we applied for the synthesis of gold nanorod dimers: (a) assembly in solution, which we can call bulk-assembly process; and (b) step-wise assembly on the surface of the substrate. The processes can be briefly described as follows.

Preparation of the molecular linkers.

A biotin disulfide solution ($20~\mu\mathrm{M}$), EZ-link HPDP-biotin, was pretreated with a reducing agent solution, TCEP (tris(2-carboxyethyl)phosphine), with a 1:10 biotin/TCEP ratio. This reaction was allowed at room temperature for 15 min to break the disulfide bonds in the HPDP-biotin molecules. This process can be verified by monitoring the extinction peak at $343~\mathrm{nm}$ [44](see figure S4.1b in Supporting Information). The mixture solution was added to the streptavidin solution ($1~\mu\mathrm{M}$) in phosphate-buffered saline solution (PBS, pH=7.4), with a ratio of 4:1 for biotin/streptavidin. The incubation lasted for 45 min to allow the binding of streptavidin with at least two biotins. The excess of unbound biotin disulfide and TCEP was removed by centrifugation in centrifugal filter devices (Ultra-0.5 10K, Amicon). The residue was dispersed in $100~\mu\mathrm{L}$ deionized (DI) water.

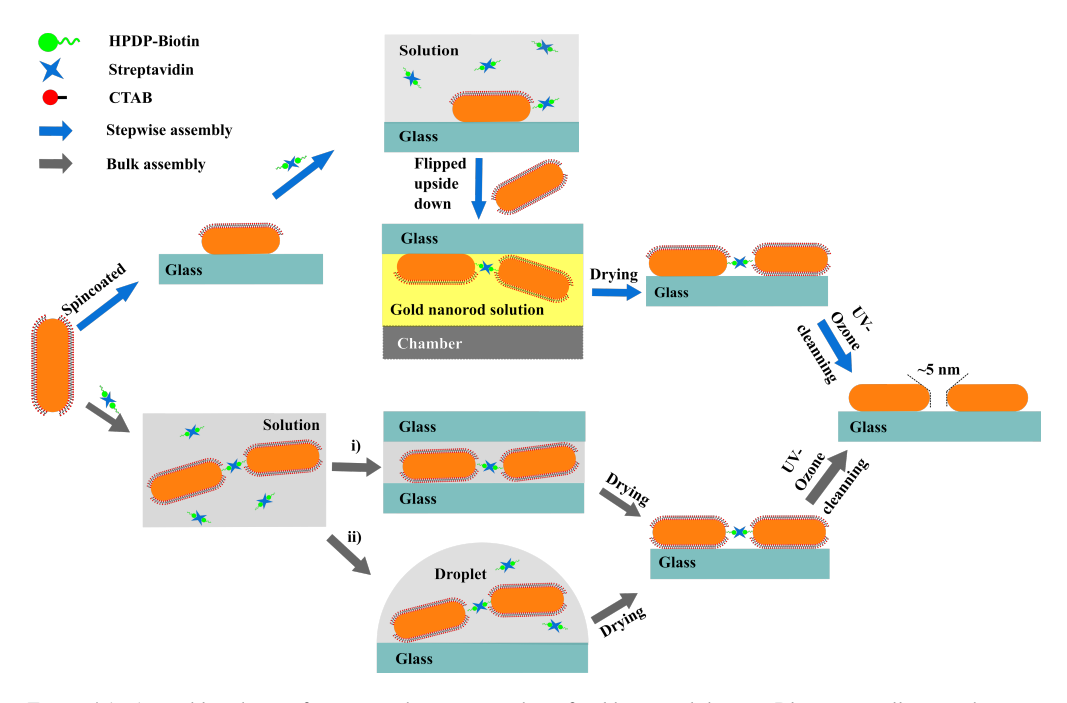


Figure 4.1: Assembly schemes for two synthesis approaches of gold nanorod dimers. Blue arrows illustrate the step-wise assembly approach where two GNRs of the dimer are immobilized sequentially on the glass surface, by spin-coating and by molecular linking, respectively. Grey arrows show the bulk-assembly approach.

(a) Step-wise assembly of GNRs on the glass surface.

Step 1. Immobilized GNRs on the glass side: Individual GNRs were immobilized onto a clean glass slide by spin-coating a suspension of CTAB-stabilized GNRs. These isolated GNRs can be viewed as the "first" GNRs of the dimers. After spin-coating, UV/Ozone cleaning was performed to remove the CTAB around GNRs' surfaces to ensure proper sticking of these GNRs on the glass surface. The slide was immersed in a CTAB solution (1 mM) for about 30 min. This step created a bilayer of CTAB that covered the sides of the GNRs more compactly, leaving the tips exposed and accessible to the thiolated molecular linkers.

Step 2. Tip-specific functionalization of the GNRs: The CTAB solution was replaced with the pretreated biotinylated streptavidin solution ($\sim 200~\mathrm{nM}$). In the presence of $\sim 1~\mathrm{mM}$ CTAB, the thiolated linkers can bind specifically at the tip of the GNRs. The tip-specific binding reaction was allowed to proceed for $90~\mathrm{min}$, and afterward the slide was cleaned gently with DI water to remove any reactant residues on the surface.

Step 3. Synthesis of GNR dimers on the glass surface: The glass slide was then flipped and immersed in GNR colloid in an upside-down manner for 12 hours, with the surface containing tip-functionalized GNRs facing the bottom of the sample chamber (see the scheme in figure 4.1). This upside-down strategy can significantly reduce the deposition of GNR monomers or aggregated multimers onto the substrate under the influence of gravity. The thiol-functionalized GNRs on the glass slide provided binding sites for the GNRs, and had the chances to "adsorb" the second GNR to form a GNR dimer through gold-thiol bonds. This step-wise assembly approach allows us to construct high-purity gold nanorod dimers on the substrate, and provides the flexibility of adjusting the shapes or sizes of each particle in the dimers.

(b) Assembly of GNRs in bulk suspension.

The assembly of GNRs can also be performed in the bulk suspension. Briefly, a commercially available GNR suspension (NA-40-700, OD-50, Nanoseedz) was diluted to the concentration according to its optical density (OD) of ~ 0.3 . The GNR suspension had plasmon absorption at 700 nm, and the average diameter of the GNRs was 40 nm. 40 μL of the pretreated biotin-streptavidin solution were added into 500 μL as-prepared GNR solution to trigger the end-to-end assembly of the GNRs. The assembly of GNRs was monitored by recording the extinction spectrum of the solution with a Cary 50 UV-Vis spectrometer (Varian Inc. Agilent Technology, USA) every $2\,\mathrm{min}$. After the extinction peak of the longitudinal plasmonic modes dropped by about 1/4, the GNR assemblies can be immobilized onto the glass slides through the following two strategies:

- i) Deposition of the GNR assemblies between two glass slides. A small amount of the GNR assembly solution ($\sim 10~\mu L)$ was deposited onto a clean cover glass slide, and was immediately covered with a second glass slide. The capillary action between the two slides squeezed the assembled solution and formed a thin layer. This strategy helps stop further assembly of GNR, and deposit the GNR assemblies uniformly on the surfaces of the glass slides. After deposition, the two slides were separated by immersing them in clean water.
- **ii) Drop-coating deposition of the GNR assemblies.** As a comparison, a traditional drop-coating approach of depositing the GNR assemblies was also examined in this study. Briefly, a small drop of GNR assembly solution was deposited on a clean glass slide, and blown dry gently with nitrogen gas.

Removing of the organic molecules around GNRs.

We performed UV/Ozone cleaning to remove all the organic molecules around the deposited GNRs to ensure the proper sticking of the GNRs on the glass surface, and to create free gaps between the GNRs of the assemblies.

4.3. Results and discussion

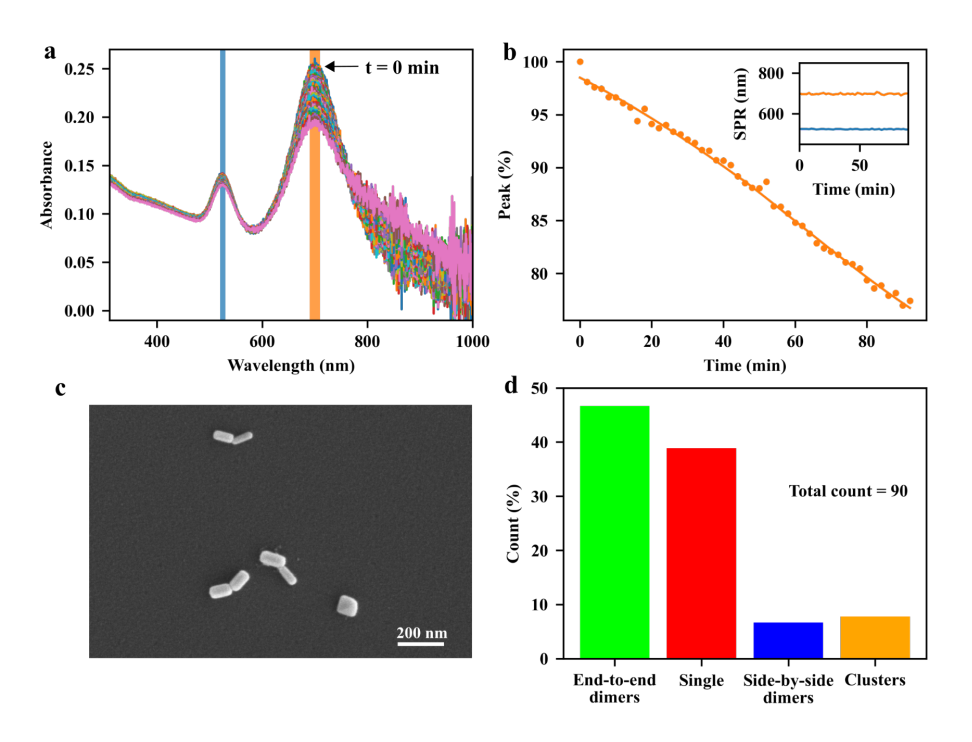


Figure 4.2: Bulk assembly experiment. (a) Spectral change during the assembly process. (b) Percentage decrease in the peak value of spectra as time progresses. The orange shaded area shown in (a) is used to calculate the normalized values. Inset: the resonance wavelenths of the transverse (blue) and longitudinal (orange) plasmon modes. (c) SEM image of typical gold nanorod dimers on glass slide deposited by using "two-slide" strategy. (d) The statistics percentages of end-to-end dimers (green), single GNRs (red), side-by-side dimers (blue), and clusters (orange). The statistics was done by counting 90 nanoparticles.

We begin our discussion with the assembly process of GNRs in the bulk suspension. As is well known, the formation of nanoparticle aggregates, or nanoparticle assemblies, can be characterized by the change of their plasmon resonances compared to single particles. The assembly process in bulk solution can be visualized by the evolution of the visible-near-infrared (vis-NIR) extinction spectra of the GNR suspension mixed with the linkers. Specifically, the elongated GNRs can be assembled side-by-side, end-to-side, or end-to-end, depending on the binding sites of the molecular linkers on the surface of each GNR. In the bulk-assembly experiments, the formation of these assemblies can be probed by monitoring the absorption bands corresponding to the transverse or longitudinal SPR of the GNRs: the

side-by-side and the end-to-side assemblies will induce a red-shift to the initial transverse SPR band of single GNRs, while the end-to-end assemblies will give rise to a red-shift of the longitudinal SPR band. The red-shifts of the plasmon modes depend on the sizes of the individual GNRs and on the gaps between them. Considering the interparticle gap of about 5 nm, determined by the size of streptavidin[39], and the average sizes $40 \text{ nm} \times 97 \text{ nm}$ of the GNRs, we expect a red-shift of about 100 nm for the longitudinal SPR of the end-to-end and a red-shift of about 30 nm for the transverse SPR of the side-by-side dimer, compared to the modes of single GNRs (see figure S4.2 in Supporting Information).

Figure 4.2a shows the evolution of the vis-NIR extinction spectra of the GNR suspension after the addition of the pretreated dithiolated streptavidin-biotin compounds. The spectra were acquired every 2 min at room temperature. After adding the molecular linkers, the extinction peak, corresponding to longitudinal SPR band of isolated GNRs, decreases gradually in intensity without shift of its spectral position, while the red-side shoulder became broader, indicating the formation of the end-to-end assemblies of GNRs in the solution. After certain time, we observed a small tail at the longer-wavelength side of the longitudinal plasmon band, which could be assigned to the increased content of the end-to-end GNR chains over time. From the spectra, we conclude that the fraction of the longer chain assemblies (e.g. the assemblies with more than three GNRs) in the solution is low, as the extinction at the end of the longer-wavelength tail is relatively small compared to the extinction at the red-side shoulder at the wavelength of around 800 nm (which corresponds to the SPR of end-to-end dimer from simulations, see figure S4.2). The ratio of short-chain assemblies (e.g. GNR dimers) can be further controlled by adjusting the assembly time and the stoichiometric ratio between GNR and the molecular linker.

From figure 4.2a, we didn't observe any noticeable change in the shape of the transverse SPR band except for a reduction of the intensity, which indicated that the GNRs assembled in the side-by-side configuration were rare in the solution. Here, the facilitation of end-toend GNR assembly can be attributed to the rigid structure of the streptavidin and of the streptavidin-biotin complexes. The relative large size of streptavidin makes it more difficult for the short thiol-end groups of the compounds to bind with the gold surfaces on the sides of the GNRs, which are coated with a CTAB layer, favoring the binding of the linkers to the GNR's tips, where the CTAB density is lower. We therefore propose that the pre-treatments of the molecular linkers mentioned earlier make them more robust to assemble the GNRs into end-to-end configurations. This statement can be confirmed by a control experiment, where we added the solutions of streptavidin, biotin and TCEP into the GNR suspension simultaneously to trigger the GNR assembly, instead of using the pre-treated solution that contained only the streptavidin-biotin compounds. Figure S4.3 shows the time-dependent extinction spectra of GNRs after the addition of the mixture of streptavidin, HPDP-biotin and TCEP, with the stoichiometric ratio of 1:4:8. As shown in the plot, the transverse SPR band was red-shifted slightly as time evolved, accompanied by an increase of the extinction at the dip of the spectra between the two SPR peaks. Hence it was evident that the GNRs could also be assembled side-by-side in the presence of free thiolated biotin and unconjugated streptavidin. Additionally, the assembly rate was faster than the assembly process with only streptavidin-biotin compouds. More controlled experiments were performed using: i) biotin and TCEP, ii) streptavidin and TCEP and iii) streptavidin-biotin linker molecules. As is shown in figure 4.3, we see that biotin-only or streptavidin-only yields negligible spectral change as time goes, compared to the case with streptavidin-biotin linker molecules.

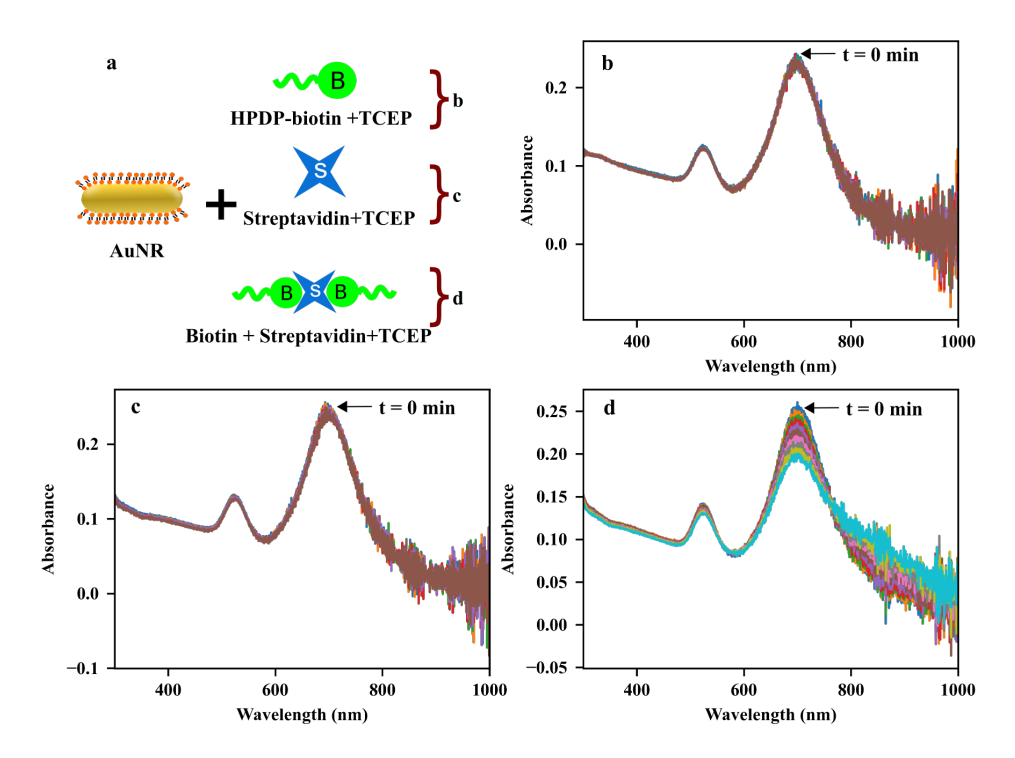


Figure 4.3: Control experiments: (a) Schematic showing the different linker molecules used for the experiment. (b, c d) Time evolution of the extinction spectra when the linker is only biotin and TCEP (b), only streptavidin and TCEP (c), and when the linker molecule is biotin-streptavidin and TCEP (d). The TCEP concentration for (b) and (c) was $100~\mu\mathrm{M}$. The spectra were acquired every $10~\mathrm{min}$ for 2 hours.

The GNR assemblies were examined via SEM measurements after deposition onto a clean glass slide. We applied the two-slide-sandwich strategy mentioned in the method section to deposit the GNR assemblies onto the glass slides. Compared to other methods, such as the drop-coating or spin-coating deposition approaches, our strategy is very simple, yet, very effective in the distribution of the assemblies on the glass surface, and can maintain the configurations of the assemblies during the deposition process. A typical SEM image of GNR dimers with well-defined end-to-end configuration is shown in figures 4.2c. More images taken from the same sample (see figure S4.5, S4.6 and S4.7 in Supporting Information) indicate that our approaches are very efficient in preparing end-to-end GNR dimers in the substrate. As shown in figures 4.2d., we obtained a ratio of 47% for the end-to-end dimers from the total count of 90 particles. More comparisons of different deposition approaches can be found in the Supporting Information.

So far we have discussed the bulk assembly approach to synthesize the end-to-end GNR dimers in GNR suspension. Our result shows that suitable treatments of the thiolated streptavidin-biotin complex facilitate the assembly of the GNRs into end-to-end configurations, which had earlier been proved by K. K. Caswell et al.[39]. Yet assembly of GNRs in bulk sus-

pension normally ends up with long chains of GNRs, and the separation of the GNR dimers from the monomers and multimers could be an issue to prepare the sample with GNR dimers on the substrate with high yields.

Inspired by the extraordinarily high affinity of streptavidn for biotin and by the chemical stability of the complex, we developed a step-wise assembly approach to synthesize GNR dimers directly on a glass surface. Briefly, the first GNR of the dimer was first immobilized on the glass surface, and later combined with the second GNR through the thiol-gold bond with the aid of the thiolated streptavidin-biotin compound functionalized at the tip of the first GNR. Similar step-wise assembly approach had been reported to create gold nanoparticle dimer with high yield by using the alkanedithiol (SH(CH₂)nSH) or double-stranded DNA as the molecular linkers[45–48]. So far, however, this strategy has only be exploited to the assembly of spherical gold nanoparticles with small sizes ($\sim 20~\rm nm$), and special functionalizations of the glass surface were needed. Here, we show that the step-wise assembly method can also be applied to fabricate GNR dimers on the substrate. By using the flipped upside-down strategy shown in figure 4.1, where the targeted GNRs were in the solution below the glass surface with tip-functionalized GNRs, we can prevent precipitation of the monomers or sedimentation of the inevitable aggregated multimers on the substrate, hence seletively bind dimer structures onto the glass surface.

Figure 4.4 shows a representative SEM image of the GNR dimers assembled using the step-wise upside-down approach. As shown in the SEM image, we got 8 GNR dimers with end-to-end configurations (noted with the green dashed circles) out of the 15 nanoparticles in the area. Meanwhile, we also see 3 particles with GNRs aggregated in the side-by-side configurations. Interestingly, we don't see any end-to-end assemblies in this area with more than three GNRs in the arrangement, which confirms that our method is effective in the fabrication of end-to-end GNR assemblies of short chains (in principle 3 GNRs at most).

Several factors could affect the efficiency of the fabrication of end-to-end dimers on the substrate by using our step-wise upside-down strategy: i) the number of the active binding sites for the targeted GNRs at the tips of the individual GNRs on the glass; ii) the denaturation of the dithiolated streptavidin-biotin complex during the assembly process; iii) the surface conditions of the glass, such as the surface roughness or the surface charge of the glass, which may influence the sticking of the second GNRs on the glass surface; iv) after taking away the glass from the GNR suspension after the assembly, there might also be some GNR suspension left on the glass surface, which might stick on the glass or even aggregate into clusters during the drying process.

We examined the SEM images in 12 different areas recorded on three different samples (including the area shown in figure 4.4) using the same method of step-wise assembly. Shown in figure S4.8 and figure S4.9, we see that the ratios of end-to-end GNR dimers can be very different in different areas. The non-uniform distribution of GNR dimers on the glass surface might be due to the non-uniform surface conditions of the glasses, which might affect the tip functionalization of each GNR, or might affect the binding efficiency of the linker with the second GNR. The random distribution of the GNR residues on the glass surface after the assembly might also affect the ratio of GNR dimer in different areas, as they will add more single GNRs on the surface. Nonetheless, we got a total of 50 end-to-end GNR dimers out of the 140 particles in all areas, which yields a ratio of 36% for end-to-end GNR dimers, as can be seen in figure 4.5 (green bar).

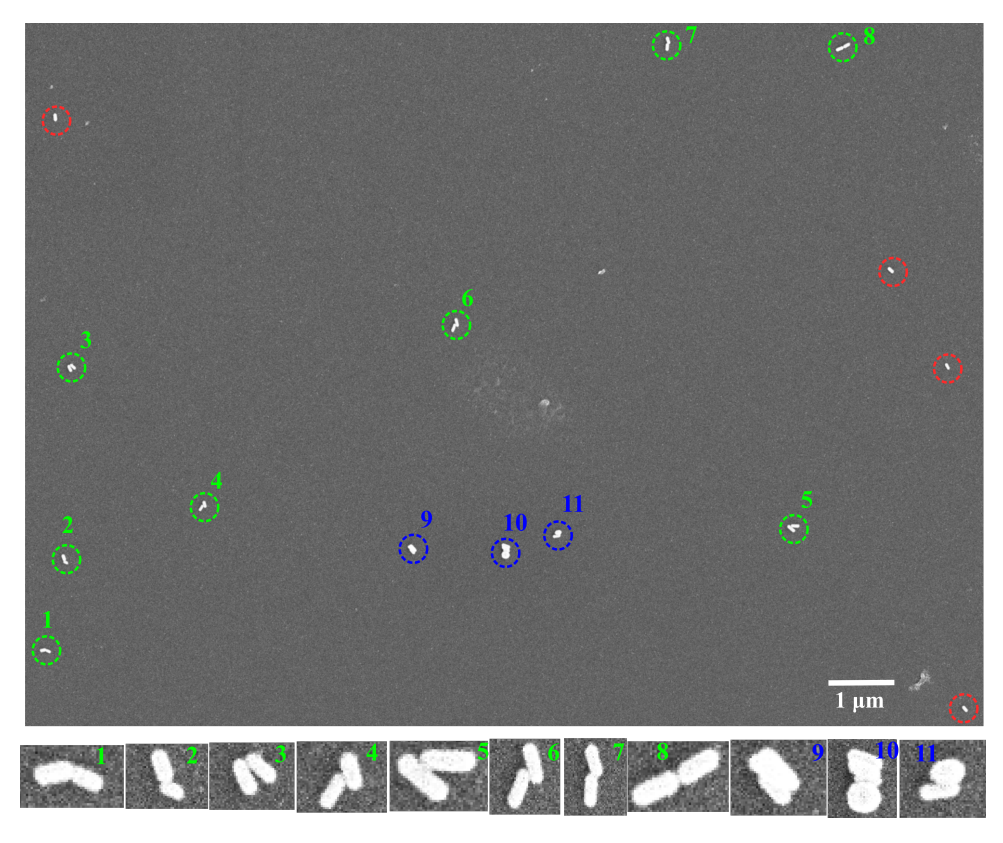


Figure 4.4: SEM image of the assembly sample prepared by using the step-wise assembly method. We see a total of 8 end-to-end GNR dimers out of 15 nanoparticles (green dashed circles) in this area. The blue and red circles represent the side-by-side assemblies and single GNRs, respectively. Below shows the zoomed in configurations of the assemblies.

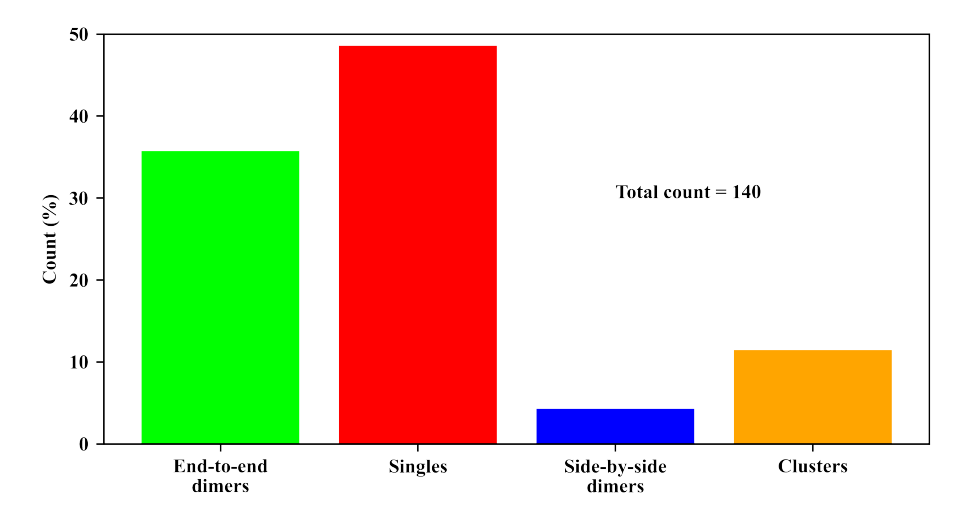


Figure 4.5: Yields of the nanoparticles with different configurations. The statistics was done by counting 140 nanoparticles from different areas of three samples, all of which were prepared by using the step-wise assembly approach.

4.4. Conclusions

In conclusion, we have demonstrated two different approaches for the fabrication of end-to-end GNR dimers based on the self-assembly of GNRs. Our results showed that pre-conjugation of streptavidin with thiolated-biotin as molecular linkers will facilitate GNR assembly into end-to-end dimers in the suspension. In this work, we illustrated a simple but very efficient way of depositing the GNR assemblies onto glass slide by sandwiching a small amount of GNR assembly between two glass slides. This approach helps us to deposit the GNR assemblies uniformly onto the glass slides, and maintain the configurations of the GNR assemblies during the deposition process.

We further developed a step-wise assembly method to synthesize GNR dimers directly on the glass. In this method, the two GNRs of the dimer were immobilized sequentially on the glass surface. Briefly, the first GNR of the dimer was immobilized by spin-coating, and adsorbed the second GNR in the suspension with the aid of the molecular linker. By applying a simple upside-down flipping strategy, where the targeted GNRs were in the solution below the glass surface with tip-functionalized GNRs, we ended up with a high yield of end-to-end GNR dimers. Our step-wise assembly method can be readily applied to different nanoparticles, providing the flexibility of controlling the shapes, sizes or materials of each nanoparticle in the assembly.

S4.1. Supporting information

GNR assembly in bulk suspension.

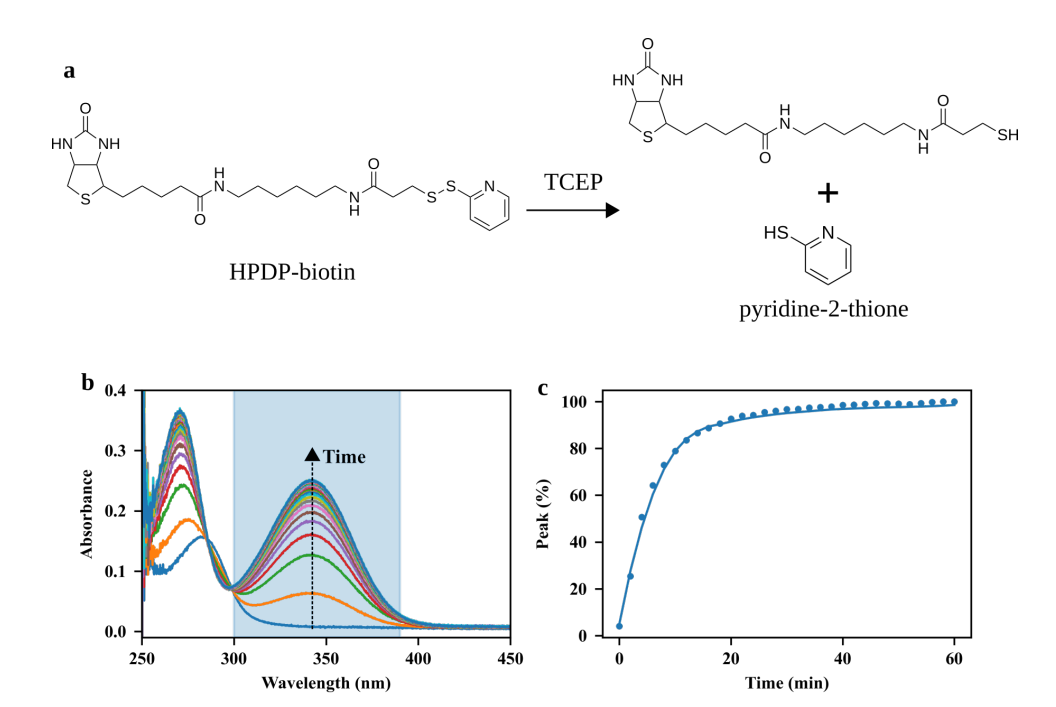


Figure S4.1: (a) Cleavage of the disulfide bond in HPDP-biotin molecule by the reducing agent TCEP. (b) Spectral evolution for HPDP-biotin at the concentration of $40~\mu\mathrm{M}$ after the addition of $40~\mu\mathrm{M}$ TCEP. The disulfide-bond cleavage of HPDP-biotin molecules is verified by monitoring the release of pyridine-2-thione, which has a maximum absorption at $343~\mathrm{nm}$. The spectra were acquired every $2~\mathrm{min}$. (b) Time evolution for the percentage of the peak at $343~\mathrm{nm}$.

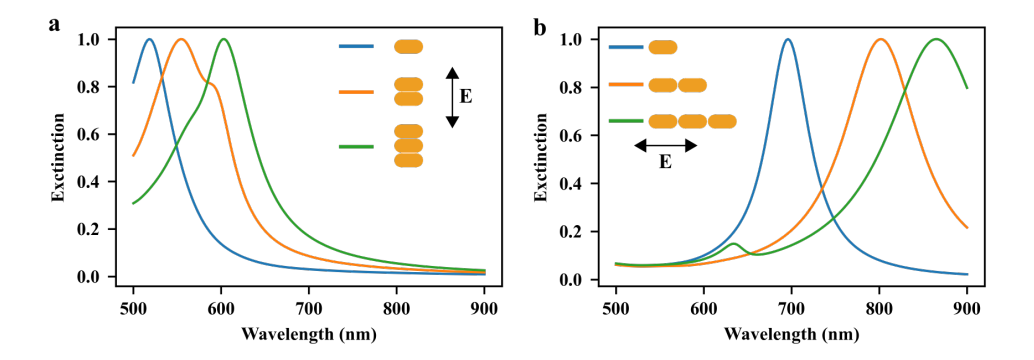


Figure S4.2: Simulated extinction spectra for GNR of different morphologies. (a) The extinction spectra excited transversely for a single GNR (blue), a side-by-side GNR dimer (orange), and a side-by-side trimer(green). (b) The extinction spectra excited longitudinally for a single GNR (blue), a end-to-end GNR dimer (orange), and a end-to-end trimer(green). Each GNR was modeled as a spherically capped clinder with the shape of $40~\rm nm \times 97~nm$. The interparticle gap was set as $5~\rm nm$. The simulations were performed by using boundary element method[49, 50]. The dielectric permitivity for gold was taken from Johnson and Christy[51], and the refractive index of ambient medium was taken as 1.33.

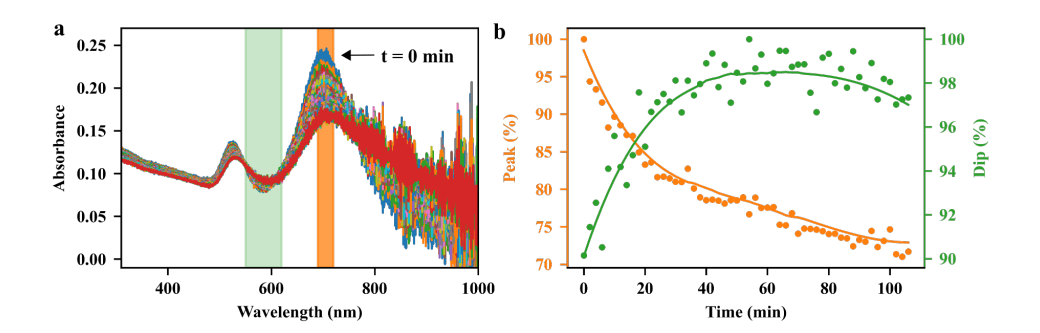


Figure S4.3: (a) Spectral evolution for GNRs in the presence of the HPDP-biotin, streptavidn, and TCEP. The assembly was triggered by adding the mixture without centrifugal filtering. (b) Time evolution of the pectcentage of the longitudinal plasmon peaks (orange line with dots), and the pectcentage of the dips (green line with dots) in the special window indicated by the green shadow in (a). The spectra were acquired every 2 min.

Drop-coating deposition of the GNR assemblies

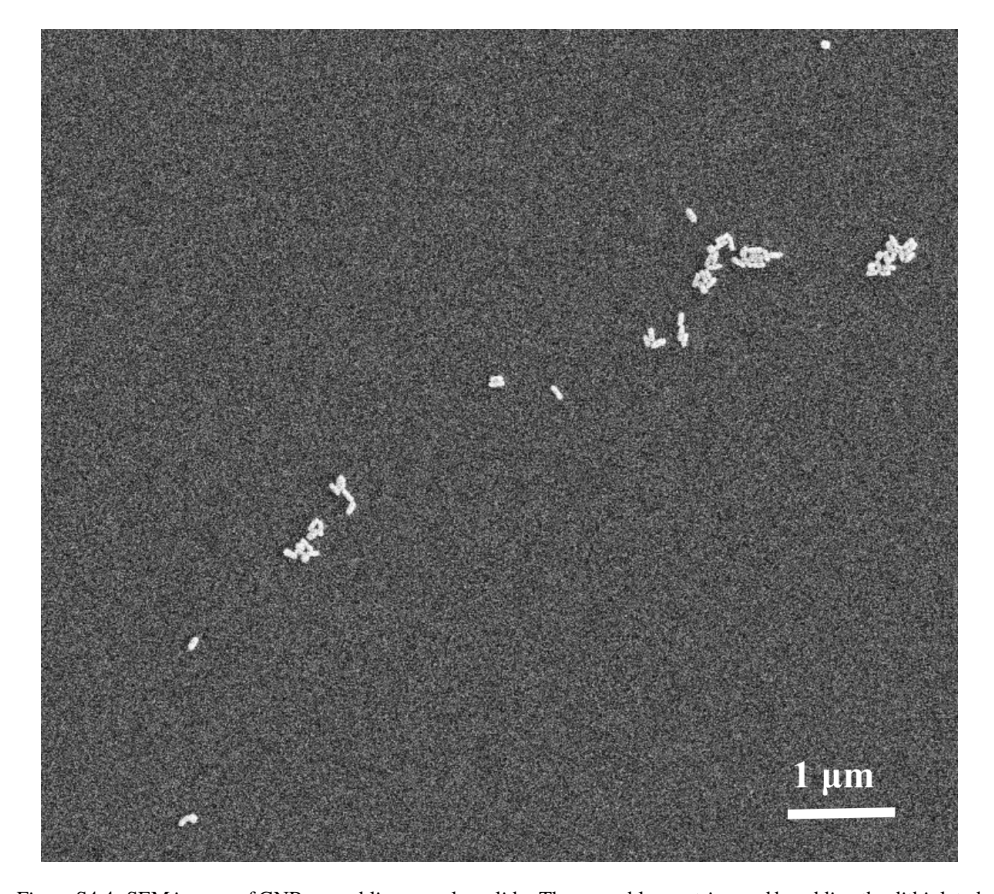


Figure S4.4: SEM images of GNR assemblies on a glass slide. The assembly was triggered by adding the dithiolated streptavidin-biotin compounds to the GNR suspension. The assemblies were deposited onto the glass slide by drop-coasting.

Deposition of the GNR assemblies between two cover slides

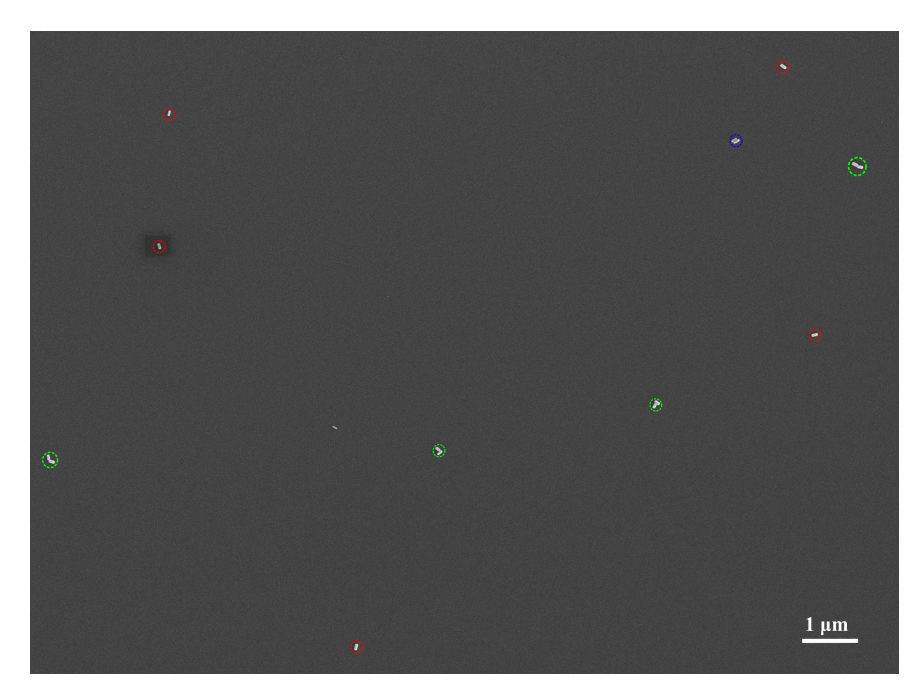


Figure S4.5: SEM images of GNR assemblies on a glass slide. The assembly was triggered by adding the dithiolated streptavidin-biotin compounds to the GNR suspension. The assemblies were deposited onto the glass slides and dried between two cover slides. The assemblies of different morphologies are highlighted by the colored circles: end-to-end GNR-dimer: green, single GNR: red, side-by-side GNR dimer: blue, and clusters: orange.

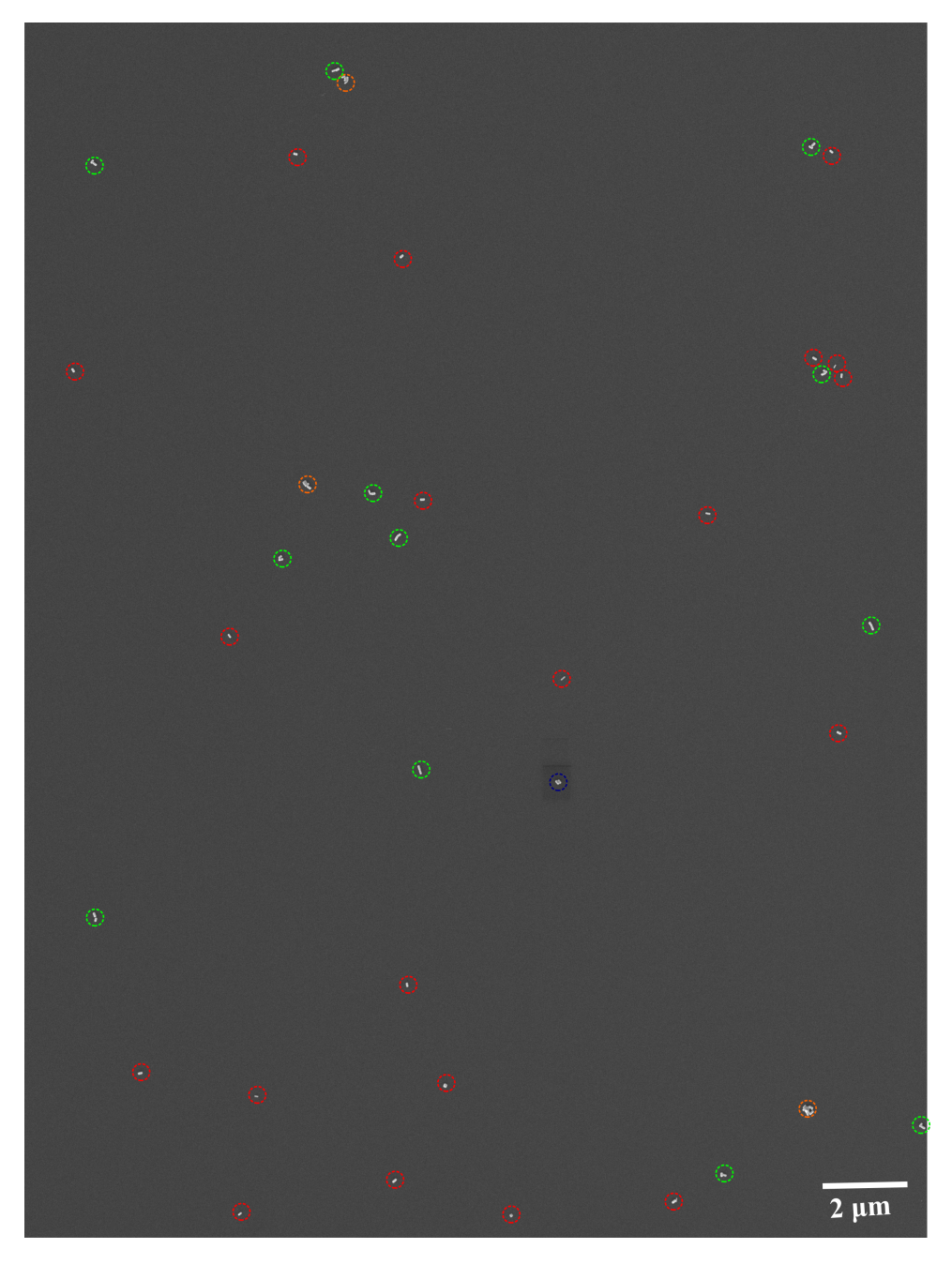


Figure S4.6: SEM images of GNR assemblies on the same glass slide as figure S4.5. The assemblies of different morphologies are highlighted by the colored circles: end-to-end GNR-dimer: green, single GNR: red, side-by-side GNR dimer: blue, and clusters: orange.

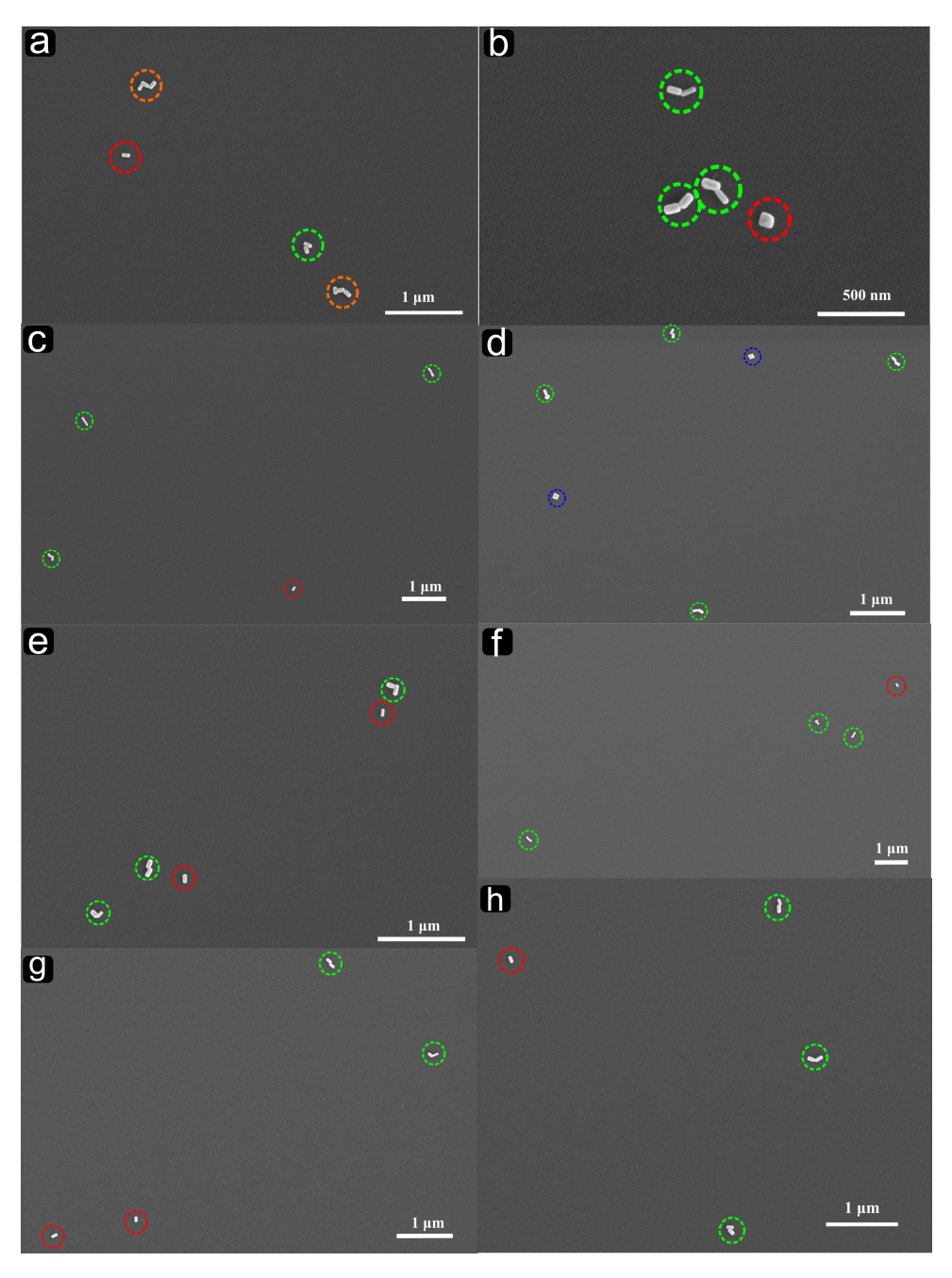


Figure S4.7: SEM images of GNR assemblies on the same glass slide as figure S4.5. (a-h) These SEM images are of different areas from the same sample. The assemblies of different morphologies are highlighted by the colored circles: end-to-end GNR-dimer: green, single GNR: red, side-by-side GNR dimer: blue, and clusters: orange.

Step-wise assembly of GNRs on the glass surface.

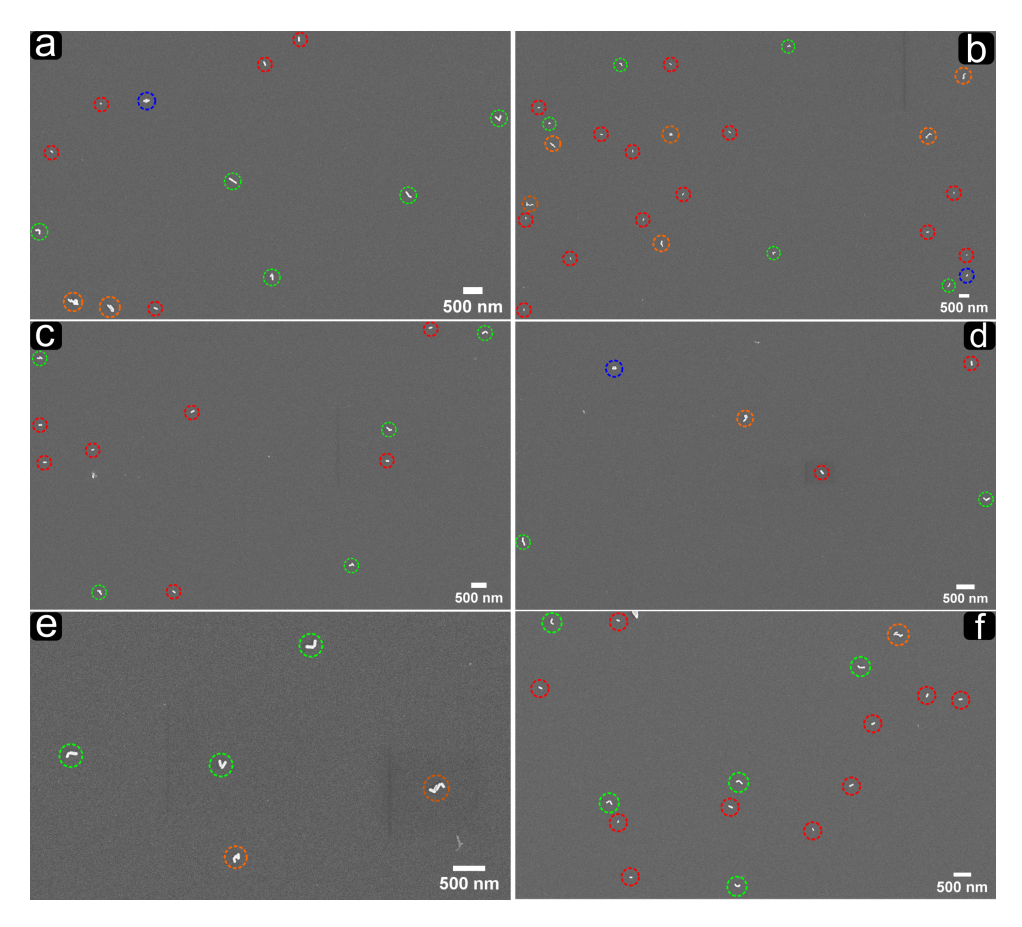


Figure S4.8: SEM images of GNR assemblies on a glass slide. The sample was prepared using the step-wise assembly method. (a-f) These SEM images are of different areas from the same sample. The assemblies of different morphologies are highlighted by the colored circles: end-to-end GNR-dimer: green, single GNR: red, side-by-side GNR dimer: blue, and clusters: orange.

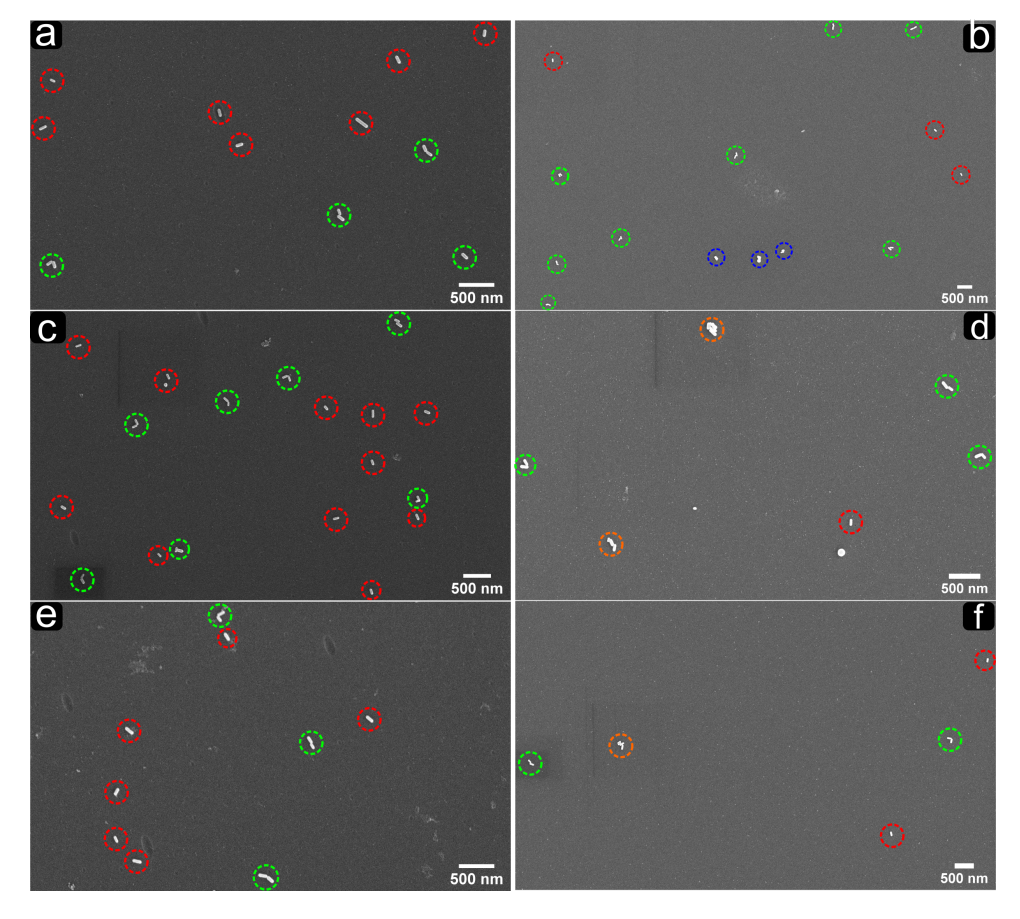


Figure S4.9: SEM images from two different samples prepared by using the step-wise assembly method. (a, c, e) Assemblies of different areas from the first sample. (b, d, f) SEM images from the second sample. The assemblies of different morphologies are highlighted by the colored circles: end-to-end GNR-dimer: green, single GNR: red, side-by-side GNR dimer: blue, and clusters: orange.

References

- [1] H. Xu, J. Aizpurua, M. Käll, and P. Apell, *Electromagnetic contributions to single-molecule sensitivity in surface-enhanced Raman scattering*, Physical Review E **62**, 4318 (2000).
- [2] A. Kinkhabwala, Z. Yu, S. Fan, Y. Avlasevich, K. Müllen, and W. E. Moerner, *Large single-molecule fluorescence enhancements produced by a bowtie nanoantenna*, Nature Photonics **3**, 654 (2009).
- [3] T. Kang, S. Hong, Y. Choi, and L. P. Lee, *The Effect of Thermal Gradients in SERS Spectroscopy*, Small **6**, 2649 (2010).
- [4] J. C. Fraire, L. A. Pérez, and E. A. Coronado, *Rational Design of Plasmonic Nanostructures for Biomolecular Detection: Interplay between Theory and Experiments*, ACS Nano **6**, 3441 (2012).
- [5] X. Lan, Z. Chen, X. Lu, G. Dai, W. Ni, and Q. Wang, *DNA-Directed Gold Nanodimers with Tailored Ensemble Surface-Enhanced Raman Scattering Properties*, ACS Applied Materials & Interfaces **5**, 10423 (2013).
- [6] P. M. R. Paulo, D. Botequim, A. Jóskowiak, S. Martins, D. M. F. Prazeres, P. Zijlstra, and S. M. B. Costa, *Enhanced Fluorescence of a Dye on DNA-Assembled Gold Nan-odimers Discriminated by Lifetime Correlation Spectroscopy*, The Journal of Physical Chemistry C 122, 10971 (2018).
- [7] L. Tie, M. Focsan, J. Bosson, C. Tira, A. Campu, A. Vulpoi, and S. Astilean, *Controlling the end-to-end assembly of gold nanorods to enhance the plasmonic response in near infrared*, **6**, 095038 (2019).
- [8] J. Langer, L. M. Liz-Marzán, et al., Present and Future of Surface-Enhanced Raman Scattering, ACS Nano 14, 28 (2020).
- [9] M. Blanco-Formoso, N. Pazos-Perez, and R. A. Alvarez-Puebla, Fabrication and SERS properties of complex and organized nanoparticle plasmonic clusters stable in solution, Nanoscale 12, 14948 (2020).
- [10] J. Zheng, X. Cheng, H. Zhang, X. Bai, R. Ai, L. Shao, and J. Wang, *Gold Nanorods: The Most Versatile Plasmonic Nanoparticles*, Chemical Reviews (2021), 10.1021/acs.chemrev.1c00422.
- [11] M. Ringler, A. Schwemer, M. Wunderlich, A. Nichtl, K. Kürzinger, T. A. Klar, and J. Feldmann, *Shaping Emission Spectra of Fluorescent Molecules with Single Plas-monic Nanoresonators*, Physical Review Letters 100, 203002 (2008).
- [12] M. P. Busson, B. Rolly, B. Stout, N. Bonod, and S. Bidault, *Accelerated single photon emission from dye molecule-driven nanoantennas assembled on DNA*, Nature Communications **3**, 962 (2012).

- [13] Z. Zhang, P. Yang, H. Xu, and H. Zheng, *Surface enhanced fluorescence and Raman scattering by gold nanoparticle dimers and trimers*, Journal of Applied Physics **113**, 033102 (2013).
- [14] A. Szenes, B. Bánhelyi, T. Csendes, G. Szabó, and M. Csete, *Enhancing Diamond Fluorescence via Optimized Nanorod Dimer Configurations*, Plasmonics **13**, 1977 (2018).
- [15] I. Kaminska, J. Bohlen, S. Mackowski, P. Tinnefeld, and G. P. Acuna, Strong Plasmonic Enhancement of a Single Peridinin–Chlorophyll a–Protein Complex on DNA Origami-Based Optical Antennas, ACS Nano 12, 1650 (2018).
- [16] O. S. Ojambati, R. Chikkaraddy, W. M. Deacon, J. Huang, D. Wright, and J. J. Baumberg, *Efficient Generation of Two-Photon Excited Phosphorescence from Molecules in Plasmonic Nanocavities*, Nano Letters **20**, 4653 (2020).
- [17] H. Chen, L. Shao, Q. Li, and J. Wang, *Gold nanorods and their plasmonic properties*, Chemical Society Reviews **42**, 2679 (2013).
- [18] P. Zijlstra, P. M. R. Paulo, and M. Orrit, *Optical detection of single non-absorbing molecules using the surface plasmon resonance of a gold nanorod*, Nature Nanotechnology **7**, 379 (2012).
- [19] W. Ni, X. Kou, Z. Yang, and J. Wang, *Tailoring Longitudinal Surface Plasmon Wavelengths, Scattering and Absorption Cross Sections of Gold Nanorods*, ACS Nano **2**, 677 (2008).
- [20] S. E. Lohse and C. J. Murphy, *The Quest for Shape Control: A History of Gold Nanorod Synthesis*, Chemistry of Materials **25**, 1250 (2013).
- [21] A. M. Funston, C. Novo, T. J. Davis, and P. Mulvaney, *Plasmon Coupling of Gold Nanorods at Short Distances and in Different Geometries*, Nano Letters **9**, 1651 (2009).
- [22] X. Lan, Z. Chen, G. Dai, X. Lu, W. Ni, and Q. Wang, *Bifacial DNA Origami-Directed Discrete, Three-Dimensional, Anisotropic Plasmonic Nanoarchitectures with Tailored Optical Chirality*, Journal of the American Chemical Society **135**, 11441 (2013).
- [23] X. Lu, J. Wu, Q. Zhu, J. Zhao, Q. Wang, L. Zhan, and W. Ni, *Circular dichroism from single plasmonic nanostructures with extrinsic chirality*, Nanoscale **6**, 14244 (2014).
- [24] M. A. Beuwer and P. Zijlstra, *Correlative microscopy of single self-assembled nanorod dimers for refractometric sensing*, The Journal of Chemical Physics **155**, 044701 (2021).
- [25] C. Li, S. Li, A. Qu, H. Kuang, L. Xu, and C. Xu, Directing Arrowhead Nanorod Dimers for MicroRNA In Situ Raman Detection in Living Cells, Advanced Functional Materials 30, 2001451 (2020).
- [26] X. Lan, X. Lu, C. Shen, Y. Ke, W. Ni, and Q. Wang, *Au Nanorod Helical Superstructures with Designed Chirality*, Journal of the American Chemical Society **137**, 457 (2015).

- [27] P. Zhan, P. K. Dutta, P. Wang, G. Song, M. Dai, S.-X. Zhao, Z.-G. Wang, P. Yin, W. Zhang, B. Ding, and Y. Ke, Reconfigurable Three-Dimensional Gold Nanorod Plasmonic Nanostructures Organized on DNA Origami Tripod, ACS Nano 11, 1172 (2017).
- [28] X. Lan, T. Liu, Z. Wang, A. O. Govorov, H. Yan, and Y. Liu, *DNA-Guided Plasmonic Helix with Switchable Chirality*, Journal of the American Chemical Society **140**, 11763 (2018).
- [29] Y. Liu, Y. Liu, and Y. Shen, *Nano-assembly and welding of gold nanorods based on DNA origami and plasmon-induced laser irradiation*, International Journal of Intelligent Robotics and Applications **2**, 445 (2018).
- [30] L. A. McCarthy, K. W. Smith, X. Lan, S. A. H. Jebeli, L. Bursi, A. Alabastri, W.-S. Chang, P. Nordlander, and S. Link, *Polarized evanescent waves reveal trochoidal dichroism*, Proceedings of the National Academy of Sciences 117, 16143 (2020).
- [31] Z. Zhao, X. Chen, J. Zuo, A. Basiri, S. Choi, Y. Yao, Y. Liu, and C. Wang, *Deterministic assembly of single emitters in sub-5 nanometer optical cavity formed by gold nanorod dimers on three-dimensional DNA origami*, Nano Research (2021), 10.1007/s12274-021-3661-z.
- [32] S. M. H. Abtahi, N. D. Burrows, F. A. Idesis, C. J. Murphy, N. B. Saleh, and P. J. Vikesland, *Sulfate-Mediated End-to-End Assembly of Gold Nanorods*, Langmuir **33**, 1486 (2017).
- [33] A. Kar, V. Thambi, D. Paital, G. Joshi, and S. Khatua, *Synthesis of Solution-Stable End-to-End Linked Gold Nanorod Dimers via pH-Dependent Surface Reconfiguration*, Langmuir **36**, 9894 (2020).
- [34] P. K. Sudeep, S. T. S. Joseph, and K. G. Thomas, *Selective Detection of Cysteine and Glutathione Using Gold Nanorods*, Journal of the American Chemical Society **127**, 6516 (2005).
- [35] Z. Sun, W. Ni, Z. Yang, X. Kou, L. Li, and J. Wang, pH-Controlled Reversible Assembly and Disassembly of Gold Nanorods, Small 4, 1287 (2008).
- [36] W. Ni, R. A. Mosquera, J. Pérez-Juste, and L. M. Liz-Marzán, *Evidence for Hydrogen-Bonding-Directed Assembly of Gold Nanorods in Aqueous Solution*, The Journal of Physical Chemistry Letters **1**, 1181 (2010).
- [37] P. Zijlstra, P. M. R. Paulo, K. Yu, Q.-H. Xu, and M. Orrit, *Chemical Interface Damping in Single Gold Nanorods and Its Near Elimination by Tip-Specific Functionalization*, Angewandte Chemie International Edition **51**, 8352 (2012).
- [38] P. M. R. Paulo, P. Zijlstra, M. Orrit, E. Garcia-Fernandez, T. C. S. Pace, A. S. Viana, and S. M. B. Costa, *Tip-Specific Functionalization of Gold Nanorods for Plasmonic Biosensing: Effect of Linker Chain Length*, Langmuir **33**, 6503 (2017).

- [39] K. K. Caswell, J. N. Wilson, U. H. F. Bunz, and C. J. Murphy, *Preferential End-to-End Assembly of Gold Nanorods by Biotin-Streptavidin Connectors*, Journal of the American Chemical Society **125**, 13914 (2003).
- [40] J. Liu, C. Kan, Y. Li, H. Xu, Y. Ni, and D. Shi, *End-to-end and side-by-side assemblies of gold nanorods induced by dithiol poly(ethylene glycol)*, Applied Physics Letters **104**, 253105 (2014).
- [41] Y. Xu, X. Wang, and X. Ma, Efficient end-to-end assembly of gold nanorods via cyclodextrin-bisphenol A based supramolecular linker, Dyes and Pigments **144**, 168 (2017).
- [42] Y. Zhu, H. Kuang, L. Xu, W. Ma, C. Peng, Y. Hua, L. Wang, and C. Xu, *Gold nanorod assembly based approach to toxin detection by SERS*, Journal of Materials Chemistry **22**, 2387 (2012).
- [43] A. F. Stewart, A. Lee, A. Ahmed, S. Ip, E. Kumacheva, and G. C. Walker, *Rational Design for the Controlled Aggregation of Gold Nanorods via Phospholipid Encapsulation for Enhanced Raman Scattering*, ACS Nano **8**, 5462 (2014).
- [44] H. Chen, H. Zou, H. J. Paholak, M. Ito, W. Qian, Y. Che, and D. Sun, *Thiol-reactive amphiphilic block copolymer for coating gold nanoparticles with neutral and functionable surfaces*, Polymer Chemistry 5, 2768 (2014).
- [45] H. Cha, J. H. Yoon, and S. Yoon, *Probing Quantum Plasmon Coupling Using Gold Nanoparticle Dimers with Tunable Interparticle Distances Down to the Subnanometer Range*, ACS Nano **8**, 8554 (2014).
- [46] D. Lee and S. Yoon, Gold Nanocube—Nanosphere Dimers: Preparation, Plasmon Coupling, and Surface-Enhanced Raman Scattering, The Journal of Physical Chemistry C 119, 7873 (2015).
- [47] H. Cha, D. Lee, J. H. Yoon, and S. Yoon, *Plasmon coupling between silver nanoparticles: Transition from the classical to the quantum regime*, Journal of Colloid and Interface Science **464**, 18 (2016).
- [48] J. Li, T.-S. Deng, X. Liu, J. A. Dolan, N. F. Scherer, and P. F. Nealey, *Hierarchical Assembly of Plasmonic Nanoparticle Heterodimer Arrays with Tunable Sub-5 nm Nanogaps*, Nano Letters **19**, 4314 (2019).
- [49] M. T. Homer Reid and S. G. Johnson, *Efficient Computation of Power, Force, and Torque in BEM Scattering Calculations*, ArXiv e-prints (2013), arXiv:1307.2966 [physics.comp-ph].
- [50] http://github.com/homerreid/scuff-EM.
- [51] P. B. Johnson and R. W. Christy, Optical Constants of the Noble Metals, Physical Review B 6, 4370 (1972).